Controllable growth and magnetic properties of nickel nanoclusters electrodeposited on the ZnO nanorod template

2009 Nanotechnology 20 495601

(http://iopscience.iop.org/0957-4484/20/49/495601)

Nanotechnology **20** (2009) 495601 (6pp) doi:10.1088/0957-4484/20/49/495601

Controllable growth and magnetic properties of nickel nanoclusters electrodeposited on the ZnO nanorod template

Yang Tang[1,2], Dongxu Zhao[1,4], Dezhen Shen[1], Jiying Zhang[1] and Xiaohua Wang[3]

[1] Key Laboratory of Excited State Processes, Changchun Institute of Optics, Fine Mechanics and Physics, Chinese Academy of Sciences, 16 East Nan-Hu Road, Open Economic Zone, Changchun 130033, People's Republic of China
[2] Graduate School of the Chinese Academy of Sciences, 19A Yuquanlu, Beijing 100049, People's Republic of China
[3] National Key Laboratory of High Power Semiconductor Laser, Changchun University of Science and Technology, 7089 WeiXing Road, ChangChun 130022, People's Republic of China

E-mail: dxzhao2000@yahoo.com.cn

Received 14 May 2009, in final form 25 July 2009
Published 6 November 2009
Online at stacks.iop.org/Nano/20/495601

Abstract
The ZnO nanorods were used as a template to fabricate nickel nanoclusters by electrodeposition. The ZnO nanorod arrays act as a nano-semiconductor electrode for depositing metallic and magnetic nickel nanoclusters. The growth sites of Ni nanoclusters could be controlled by adjusting the applied potential. Under −1.15 V the Ni nanoclusters could be grown on the tips of ZnO nanorods. On increasing the potential to be more negative the ZnO nanorods were covered by Ni nanoclusters. The magnetic properties of the electrodeposited Ni nanoclusters also evolved with the applied potentials.

1. Introduction

As a wide bandgap semiconductor, ZnO nanostructures have been the focus of theoretical and experimental efforts worldwide in recent years because of their potential applications as ultraviolet lasers [1], field-effect transistors [2], gas sensors [3], field-emission displays [4] and nanogenerators [5, 6]. Different methods were used to fabricate ZnO nanostructures. Among them the template-induced growth method was a popular method. Various templates, including anodic aluminum oxide (AAO) [7–12], patterned ZnO thin films [13], porous silicon [14, 15], etc, have been adopted to fabricate ZnO nanostructures. Actually the as-grown ZnO nanostructure itself could also act as a template to prepare other kinds of nanostructures. But there have been few reports about this. In 2006, Yang *et al* used ZnO nanowires as the template to fabricate vertical aligned GaN nanotubes [16].

In this paper we used ZnO nanorods as templates to guide the nickel nanocluster growth. As an important transitional metal, nickel has attracted a great deal of attention in terms of its expected applications in high-density magnetic recording or magnetic sensors, catalysis and Ni-based batteries [17–20]. The fabrication of magnetic materials/semiconductor heterostructures is of particular interest in nanoscale spintronics [21]. The electrochemical techniques were used to grow ZnO nanostructures and Ni nanoclusters. By adjusting the growth parameters, such as the applied potentials and growth time, we realized the controllable growth sites of Ni nanoclusters on ZnO nanorods. It is expected that the ability to grow tunable magnetic-metal/semiconductor nanorod heterostructures can increase the versatility and power of these building blocks for applications in nanoscale spintronics [21]. As a low temperature process, electrodeposition can avoid interdiffusion and compound formation at the interfaces so that an abrupt

[4] Author to whom any correspondence should be addressed.

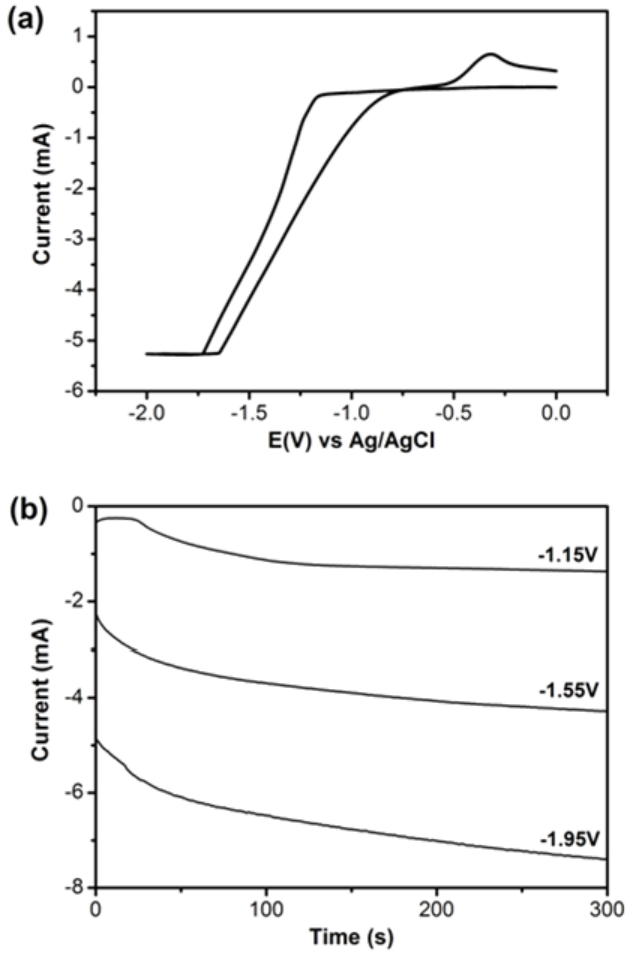

Figure 1. (a) Cyclic voltammogram for the electrodeposition of nickel on ZnO nanorods at a scan rate of 20 mV s^{-1} (solution contains 0.01 M $Ni(CH_3COO)_2$ and 0.05 M CH_3COONH_4). (b) Current–time transients for the electrodeposition of Ni on ZnO nanorods under deposition potential between −1.15 and −1.95 V (versus Ag/AgCl).

and clean interface could be created, which is necessary for the injection of spin-polarized currents from the ferromagnet to the semiconductor [22]. The Ni-covered ZnO nanorods, which are a radial structure, namely nanocables, can provide a more efficient injection current with respect to the crossed and the axial structures [23, 24]. Chen *et al* reported that the magnetoelectric coupling in the Ni–Fe alloy/ZnO nanorod composites was greatly enhanced due to the large surface-to-volume ratio of the nanorods and the avoidance of the substrate clamping effect [25]. In addition, magnetic fields have been used to control the direction and the position of magnetic nanowires and Ni end-capped nonmagnetic nanowires recently [26–28]. Thus it is expected that Ni end-capped or covered ZnO nanorods can be applied to make a matrix of devices as well as a single device using magnetic alignment.

2. Experimental methods

Indium tin oxide glasses (ITO) were used as substrates in all the experiments in this paper. After ultrasonic cleaning in acetone and alcohol, the wafers were rinsed with deionized water, then transferred to the electrodeposition cell with a Pt counter-electrode and an Ag/AgCl reference electrode. The ZnO nanorods on ITO were prepared from aqueous electrolytes containing $Zn(NO_3)_2$ and hexamethylenamine ($C_6H_{12}N_4$) at 90 °C. The applied potential was −0.8 V and the deposition time was 1 h. The ZnO nanorod has an approximate length of 1 μm with a diameter around 150 nm.

After the electrodeposition of ZnO nanorods, the sample was pulled out and dried. The electrodeposition of Ni nanoclusters was carried out at a constant potential of −1.150 V at room temperature using 0.01 M $Ni(CH_3COO)_2$ as the source material and 0.05 M CH_3COONH_4 as the supporting electrolyte. The growth parameters, such as the applied potentials of the deposition and growth time, were intentionally changed in order to investigate the influence of different growing conditions on the morphologies of as-grown samples. The surface morphology of the nanostructures was observed by a field-emission scanning electron microscopy (FESEM, Hitachi S-4800). Magnetic characteristics were studied using a vibrating sample magnetometer (VSM) (Lake Shore Co.) at room temperature.

3. Results and discussion

Cyclic voltammetry (CV) experiments was made from the solution containing 0.01 M $Ni(CH_3COO)_2$ and 0.05 M CH_3COONH_4 with ZnO nanorods grown on ITO as the working electrode (scan rate 20 mV s^{-1}). When the substrate potential was scanned cathodically, a current peak for the reduction of Ni^{2+} to Ni was observed at −1.15 V versus an Ag/AgCl reference electrode as shown in figure 1(a). At this potential, Ni nucleation started on the template and served to catalyze the evolution of H_2 [29]. The peak observed at −0.33 V on scanning in the positive direction is due to the oxidation of nickel. To determine the effect of different applied potentials on Ni particles' deposition on ZnO nanorods, current versus time (I–t) transients are shown in figure 1(b). At the lower potential (−1.15 V), after an initial charging decay, the current rises on increasing the time. The charge decay process is due to the individual diffusion fields not overlapping, because the initial growth of Ni nanoclusters is sufficiently small and well separated. Then the Ni nanoclusters may grow in size or increase in number, so that the current increases [30]. As the applied potential turns more cathodic, the initial current transition occurs in a much shorter timescale, so that the I–t characteristics show that the current continually increases on increasing the time. The currents are rather greater than that at −1.15 V, which is caused both by an increased deposition rate of Ni nanoclusters and by an accelerated H_2 evolution [29].

Figure 2(a) shows the SEM image of a uniform Ni thin film electrodeposited directly on ITO under −1.15 V for 1 min from 0.01 M $Ni(CH_3COO)_2$ and 0.05 M CH_3COONH_4 at room temperature. The substrate surface is entirely covered by the compact Ni films. Figures 2(b) and (c) show the SEM images of Ni nanocluster electrodeposition on ZnO nanorods at −1.15 V for 10 min. It could be observed that some Ni nanoclusters were mainly grown on the tips of ZnO nanorods.

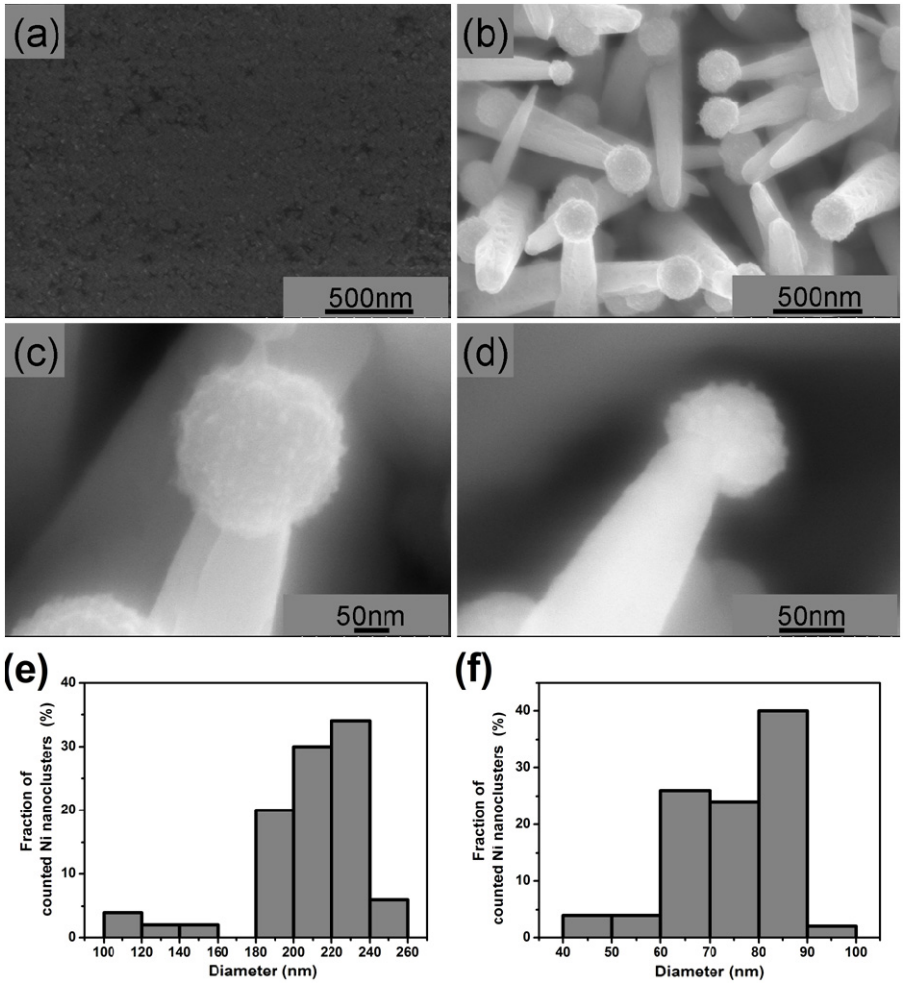

Figure 2. (a) SEM images of Ni thin films electrodeposited on ITO under −1.15 V for 1 min, (b)–(d) Ni nanoclusters electrodeposited on ZnO nanorods under −1.15 V. (e), (f) The size dispersion of the Ni nanoclusters. The growth time is 10 min for (b), (c) and (e) and 5 min for (d) and (f).

The Ni cluster caps, which consisted of smaller Ni nanoclusters with diameters of several nanometers, have a spheroid shape and the typical diameter of the Ni cap is approximately 200 nm. The diameter distribution was shown in figures 2(e) and (f). With the growth time decreasing to 5 min, the size of Ni clusters deposited on ZnO nanorods decreases to 80 nm, as shown in figures 2(d) and (f).

But with decreasing cathodic potential to −1.55 V, the deposited Ni nanoclusters almost cover the whole surface of ZnO nanorods shown in figures 3(a) and (b), which indicates that the density of Ni nucleation on ZnO nanorods greatly increases at a larger applied potential. Figures 3(c) and (d) show the Ni morphology electrodeposited on ZnO nanorods at −1.95 V. The ZnO nanorods are also completely covered by Ni deposits. The morphologies in figures 2 and 3 show that the quantities of Ni nanoclusters are increasing on making the potential more cathodic. Also the sites of Ni nanoclusters on ZnO nanorods are affected by the applied potential. For the lower potential of −1.15 V, the electric potential on the tip of the ZnO nanorods is much larger than at the surface because of the small radius in the initial charge decay process. Therefore, the Ni^{2+} ions in the solution are first reduced on the tip of ZnO nanorods to form a nucleation site for Ni nanocluster growth. But with greater cathodic potential the charge decay process was shortened a lot. The electric field could be dispersed on the surfaces of ZnO nanorods in a short time, which resulted in the whole surface of ZnO releasing the electrons and reducing the Ni^{2+} ions. Due to this reason Ni nanoclusters were mainly grown on the tips of ZnO nanorods under the applied potential of −1.15 V. Additionally, the ZnO nanorods in the electrodeposition process can be viewed as nano-electrode arrays. The electrodeposition process is a complex multi-step procedure. The changes in the electrolyte bulk phase and the electrode interface are continuous during the deposition process. In our previous report NH_4^+ ions in the electrolyte play a role assisting the Ni deposition [31]. The Ni^{2+} and its ammonium group complex in the electrolytes transfer to the vicinity of the electrode interface. The ions discharge at the interface and then generate the absorbed atoms. The Ni electrodeposition process in the electrolyte is as follows [32]:

$$[Ni(NH_3)_2]^{2+} = Ni^{2+} + 2NH_3 \quad (1)$$

$$Ni^{2+} + 2e^- \rightarrow Ni \quad (2)$$

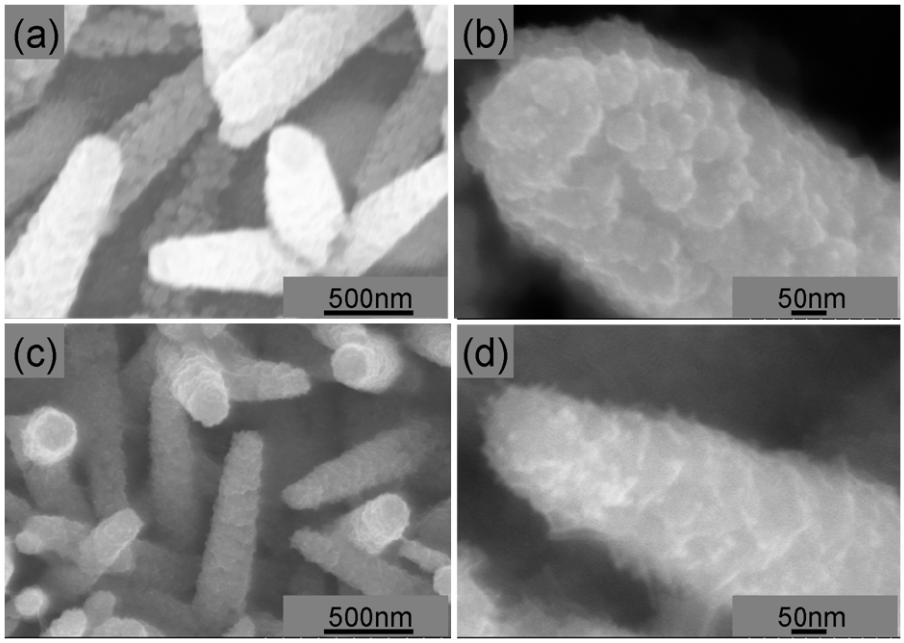

Figure 3. SEM images of Ni nanoclusters electrodeposited on ZnO nanorods for 5 min. The applied cathode potential is −1.55 V for (a) and (b) and −1.95 V for (c) and (d).

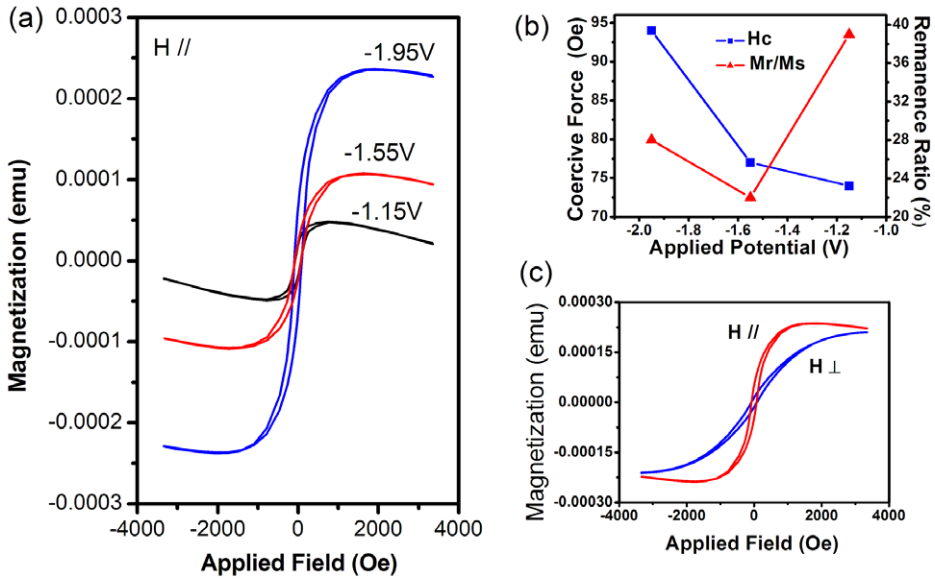

Figure 4. (a) VSM hysteresis loop for Ni nanoclusters on ZnO nanorods electrodeposited for 5 min under the deposition potential between −1.15 and −1.95 V. The magnetic field was applied parallel to the substrate surface. (b) The dependence of coercive force and remanence ratio of Ni/ZnO nanostructures on the cathode potential. (c) VSM hysteresis loop for Ni nanoclusters on ZnO nanorods electrodeposited for 10 min under −1.15 V. The magnetic field was applied parallel and perpendicular to the substrate surface.
(This figure is in colour only in the electronic version)

$$NH_3 + H_2O = NH_4^+ + OH^- \quad (3)$$

$$Ni^{2+} + 2OH^- \rightarrow Ni(OH)_2 \quad (4)$$

$$Ni(OH)_2 + 2e^- \rightarrow Ni + 2OH^-. \quad (5)$$

Under a low negative deposition potential (−1.15 V), the reactions are along this path ((1) → (3) → (4) → (5)) [32]. The transitional product $Ni(OH)_2$ preferentially grows on the top surfaces of the ZnO nanorods and is then decomposed into Ni clusters. A high negative potential (−1.55 or −1.95 V) will make the reactions go along the other path ((1) → (2)), which results in the disappearance of the preferential growth and the Ni clusters cover the whole surface of the ZnO nanorods.

Figure 4(a) shows the room temperature hysteresis loops of Ni nanoclusters electrodeposited on ZnO nanorods under different potentials. The applied magnetic field was parallel

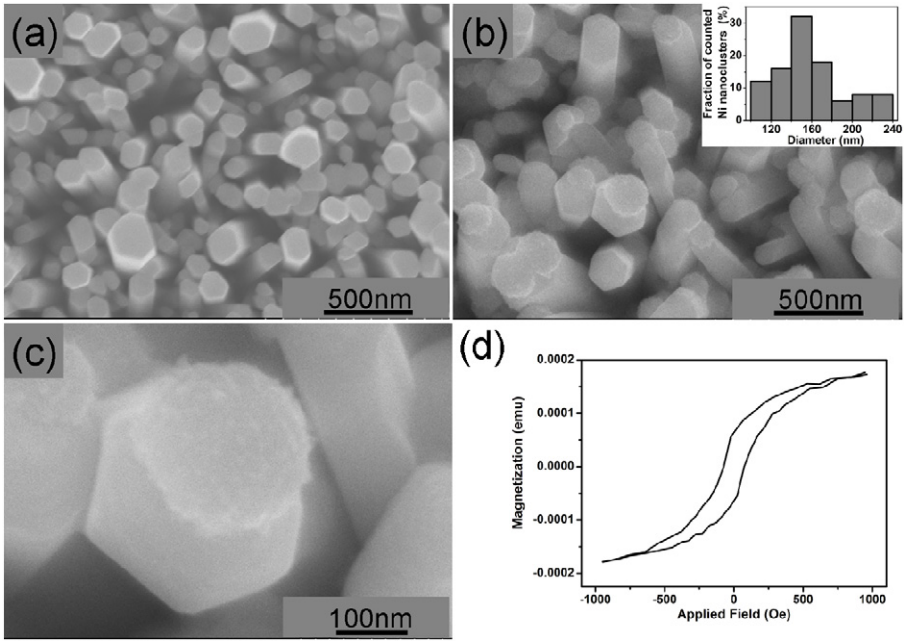

Figure 5. (a) SEM images of vertically aligned ZnO nanorods by hydrothermal method; (b)–(d) Ni nanoclusters electrodeposited on vertically aligned ZnO nanorods under −1.15 V for 5 min. The inset image in (b) shows the size dispersion of the Ni nanoclusters. (d) VSM hysteresis loop for Ni nanoclusters on vertically aligned ZnO nanorods.

to the surfaces of the samples. The coercive forces (H_c) are 74 Oe, 77 Oe and 94 Oe for deposition potentials of −1.15 V, −1.55 V and −1.95 V, respectively. The remanence ratios (ratio of remanent magnetization (M_r) to saturation magnetization (M_s)) are 39%, 22% and 28%, indicated in figure 4(b). The coercive force of the Ni nanoclusters deposited under −1.15 V is comparable with that deposited under −1.55 V. The remanence of Ni nanoclusters grown under −1.15 V is larger than those under more cathodic deposition potential, showing that Ni end-capped ZnO nanorods are more easily magnetized than the Ni-covered ZnO nanorods when the deposition time is kept to 5 min. The coercive force and remanence of the Ni-covered ZnO nanorods were enhanced from 77 Oe and 22% to 94 Oe and 28% on increasing the applied potential from −1.55 to −1.95 V during the process of Ni electrodeposition. The deposited Ni nanoclusters grown under −1.55 V almost covered the whole surface of ZnO nanorods and the Ni nanoclusters under −1.95 V covered the surfaces of the ZnO nanorods completely. The density of the Ni nanoclusters deposited on the ZnO nanorods under −1.95 V was larger than that under −1.55 V, indicating that the surface-to-volume ratio of the Ni layer was decreased. The enhanced magnetization is attributed to the decreasing of the Ni surface-to-volume ratio, since the surface region leads to a decrease in the effective magnetic moment. Similar behavior has been observed in Ni-coated ZnO nanorod heterostructures, the coercive force and remanence of which were promoted by increasing the thickness of the Ni layer [21]. The coercive force (94 Oe) of the Ni nanocluster deposited under −1.95 V is comparable with that of the bulk microcrystalline Ni (100 Oe) [33]. Figure 4(c) shows the hysteresis loops of Ni nanoclusters electrodeposited on ZnO nanorods for 10 min under −1.15 V, while the applied magnetic field is parallel and perpendicular to the sample surface, respectively. The coercive force and remanence ratio are 75 Oe and 21% when the magnetic field is parallel to the sample surface, and 83 Oe and 7% when the applied field is perpendicular to the surface. The coercive force of the Ni nanoclusters grown for 10 min is comparable with that of the Ni nanoclusters grown for 5 min. Because Ni exhibits a small magnetocrystalline anisotropy, the magnetic response is dominated by the shape anisotropy [34]. It is reported that electrodeposited Ni films have a strong shape anisotropy exhibiting characteristics of an easy magnetized axis ($M_r/M_s = 0.67$) while the applied magnetic field is parallel to the film plane and characteristic of a hard magnetized axis (smaller than 0.02), while the applied field is perpendicular to the film plane [34]. However, the Ni nanoclusters in this paper exhibit more isotropic characteristics (much smaller contrast of the remanences under parallel and perpendicular magnetic fields) than the electrodeposited Ni films. This is attributed to the isotropic spherical structure of the Ni nanoclusters electrodeposited on ZnO nanorods. The more isotropic behavior in magnetic response has also been observed in an Ni hollow sphere array [35].

In addition, the vertically aligned ZnO nanorod arrays have been used as the templates. The ZnO nanorod arrays were fabricated on ITO substrates by the hydrothermal method. A ZnO seed layer was pre-coated on ITO by electron beam evaporation. The reaction solution was prepared by mixing 0.05 M $Zn(NO_3)_2$ and 0.05 M $C_6H_{12}N_4$ aqueous solutions. The hydrothermal growth was carried out at 90 °C in a Teflon vessel placed in a sealed kettle by immersing the substrates vertically into the reaction solution. The reaction time was 20 h. Subsequently, the substrates were washed with deionized water and dried in air. Figure 5(a) illustrates the morphology of the as-grown ZnO nanorod arrays: the rods are oriented

in a vertical direction with diameters ranging from 100 to 200 nm. After Ni electrodeposition on the nanorod arrays at −1.15 V for 5 min from 0.01 M $Ni(CH_3COO)_2$ and 0.05 M CH_3COONH_4, Ni nanoclusters can be observed mainly on the top of ZnO nanorods as shown in figure 5(b). The diameter distribution of Ni nanoclusters was shown in the inset image. Ni nanoclusters with spheroid shapes were grown on top of the ZnO nanorods indicated in figure 5(c). Figure 5(d) shows the room temperature hysteresis loops of Ni nanoclusters electrodeposited on vertically aligned ZnO nanorod arrays. The applied magnetic field is parallel to the surfaces of the samples. The coercive force (H_c) of the Ni nanoclusters is 74 Oe and the remanence ratio is 36%, which are comparable with those deposited on unorderly oriented ZnO nanorods.

4. Conclusion

In summary, the Ni nanoclusters were electrodeposited on ZnO nanorod arrays at room temperature. Under −1.15 V the Ni nanoclusters were mainly grown on the tips of ZnO nanorods. With greater cathodic potentials, the Ni nanoclusters were deposited covering the whole ZnO nanorod surface. The Ni end-capped ZnO nanorods exhibit more remanence and less anisotropy in magnetic response than electrodeposited Ni films. It is expected that the Ni end-capped and covered ZnO nanorods may have potential applications in nanoscale spintronics and manipulation of nanorods under magnetic fields.

Acknowledgments

This work is supported by the Key Project of the National Natural Science Foundation of China under grant nos. 60336020 and 50532050, the '973' program under grant no. 2006CB604906, the CAS Innovation Program, and the National Natural Science Foundation of China under grant nos. 60429403, 60506014, 50402016 and 10674133.

References

[1] Huang M H, Mao S, Feick H, Yan H, Wu Y, Kind H, Weber E, Russo R and Yang P 2001 *Science* **292** 1897
[2] Wang X, Zhou J, Song J, Liu J, Xu N and Wang Z L 2006 *Nano Lett.* **6** 2768
[3] Arnold M S, Avouris P, Pan Z W and Wang Z L 2003 *J. Phys. Chem.* B **107** 659
[4] Lee C J, Lee T J, Lyu S C, Zhang Y, Ruh H and Lee H J 2002 *Appl. Phys. Lett.* **81** 3648
[5] Wang Z L and Song J 2006 *Science* **312** 242
[6] Wang X, Song J, Liu J and Wang Z L 2007 *Science* **316** 102
[7] Li Y, Meng G W, Zhang L D and Phillipp F 2000 *Appl. Phys. Lett.* **76** 2011
[8] Liu C H, Zapien J A, Yao Y, Meng X M, Lee C S, Fan S S, Lifshitz Y and Lee S T 2003 *Adv. Mater.* **15** 838
[9] Zheng M J, Zhang L D, Li G H and Shen W Z 2002 *Chem. Phys. Lett.* **363** 123
[10] Chen W, Tao X, Liu Y, Sun X, Hu Z and Fei B 2006 *Appl. Surf. Sci.* **252** 8683
[11] Zhao A, Liang J, Xiong Z and Qian Y 2007 *Chem. Lett.* **36** 432
[12] Yang C-J, Wang S-M, Liang S-W, Chang Y-H, Chen C and Shieh J M 2007 *Appl. Phys. Lett.* **90** 033104
[13] Conley J F Jr, Stecker L and Ono Y 2005 *Nanotechnology* **16** 292
[14] Hsu H-C, Cheng C-S, Chang C-C, Yang S, Chang C-S and Hsieh W-F 2005 *Nanotechnology* **16** 297
[15] Chang C-C and Chang C-S 2004 *Japan. J. Appl. Phys.* **43** 8360
[16] Goldberger J, Fan R and Yang P 2006 *Acc. Chem. Res.* **39** 239
[17] Liu Q, Liu H, Han M, Zhu J, Liang Y, Xu Z and Song Y 2005 *Adv. Mater.* **17** 1995
[18] Jin P, Chen Q, Hao L, Tian R, Zhang L and Wang L 2004 *J. Phys. Chem.* B **108** 6311
[19] Wang D, Song C, Hu Z and Fu X 2005 *Phys. Chem.* B **109** 1125
[20] Bao J, Liang Y, Xu Z and Si L 2003 *Adv. Mater.* **15** 1832
[21] Jung S W, Park W I, Yi G-C and Kim M 2003 *Adv. Mater.* **15** 1358
[22] Evans P, Scheck C, Schad R and Zangari G 2003 *J. Magn. Magn. Mater.* **260** 467
[23] Fukumura T, Jin Z, Ohtomo A, Koinuma H and Kawasaki M 1999 *Appl. Phys. Lett.* **75** 3366
[24] Wang D, Park S, Lee Y, Eom T, Lee S, Lee Y, Choi C, Li J and Liu C 2009 *Cryst. Growth Des.* **9** 2124
[25] Chen Y C, Cheng C L, Liou S C and Chen Y F 2008 *Nanotechnology* **19** 485709
[26] Tanase M, Silevitch D M, Hultgren A, Bauer L A, Searson P C, Meyer G J and Reich D H 2002 *J. Appl. Phys.* **91** 8549
[27] Bentley A K, Trethewey J S, Ellis A B and Crone W C 2004 *Nano Lett.* **4** 487
[28] Lee S-W, Jeong M-C, Myoung J-M, Chae G-S and Chung I-J 2007 *Appl. Phys. Lett.* **90** 133115
[29] Zach M P and Penner R M 2000 *Adv. Mater.* **12** 878
[30] Day T M, Unwin P R and Macpherson J V 2007 *Nano Lett.* **7** 51
[31] Tang Y, Zhao D, Shen D, Zhang J, Li B, Lu Y and Fan X 2008 *Thin Solid Films* **516** 2094
[32] Duan G, Cai W, Luo Y, Li Z and Lei Y 2006 *J. Phys. Chem.* B **110** 15729
[33] Hwang J H, Dravid V P, Teng M H, Host J J, Elliott B R, Johnson D L and Mason T O 1997 *Mater. Res.* **12** 1076
[34] Eagleton T S and Searson P C 2004 *Chem. Mater.* **16** 5027
[35] Duan G, Cai W, Li Y, Li Z, Cao B and Luo Y 2006 *J. Phys. Chem.* B **110** 7184